IGRT/ART phantom with programmable independent rib cage and tumor motion

Haas, O.C.L. , Mills, J.A. , Land, I. , Mulholl, P. , Menary, P. , Crichton, R. , Wilson, A. , Sage, J. , Anna, M. and Depuydt, T.

Original citation & hyperlink:
Haas, O.C.L. , Mills, J.A. , Land, I. , Mulholl, P. , Menary, P. , Crichton, R. , Wilson, A. , Sage, J. , Anna, M. and Depuydt, T. (2014) IGRT/ART phantom with programmable independent rib cage and tumor motion. Medical Physics, volume 41 (2): 022106.
http://dx.doi.org/10.1118/1.4860662

IGRT/ART phantom with programmable independent rib cage and tumour motion

Olivier C L Haas

O.HAAS@COVENTRY.AC.UK

+44 2477659189

Control Theory and Applications Centre, Coventry University, Coventry, CV1 2TL, UK

John A Mills, Imke Land, Pete Mulholl, Paul Menary, Robert Crichton, Adrian Wilson, John Sage

Department of Clinical Physics & Bioengineering, University Hospital, Coventry, CV2 2DX, UK

Morenc Anna

University Hospitals of Leicester NHS Trust of Infirmary Square, Leicester, LE1 5WW, UK

Tom Depuydt

Radiotherapy, Medical Physics Group, University Hospital UZ Brussel, Laarbeeklaan 101 - 1090 Brussels, Belgium

Abstract

Purpose: This paper describes the design and experimental evaluation of the MAESTRO thorax phantom, a new anthropomorphic moving ribcage combined with a 3D tumour positioning system to move target inserts within static lungs. Material and Method: The new rib cage design is described and its motion evaluated using Vicon Nexus, a commercial 3D motion tracking system. CT studies at inhale and exhale position are used to study the effect of rib motion and tissue equivalence. Results: The 3D target positioning system and the rib cage have millimetre accuracy. Each axis of motion can reproduce given trajectories from files or individually programmed sinusoidal motion in terms of amplitude, period and phase shift. The maximum rib motion ranges from 7 to 20 mm SI and from 0.3 to 3.7 mm AP with LR motion less than 1 mm. The repeatability between cycles is within 0.16 mm RMSE. The agreement between CT electron and mass density for skin, ribcage, spine hard and inner bone as well as cartilage is within 3%. Conclusions: The MAESTRO phantom is a useful research tool that produces programmable 3D rib motions which can be synchronised with 3D internal target motion. The easily accessible static lungs enable the use of a wide range of inserts or can be filled with lung tissue equivalent and deformed using the target motion system.

Key words: Radiotherapy phantom, IGRT, ART, thorax, rib cage, Vicon, ribs, spine, skin, motion management

I. INTRODUCTION

IGRT and ART phantoms are used in radiotherapy to evaluate respiration induced external/internal motion correlation and prediction as well as the accuracy of radiotherapy equipment enabling the latter to deliver the appropriate dose at the correct instant in time. The timing and accuracy of the treatment delivery is particularly relevant in intensity modulation using photons or scanned protons beams which exhibit sharp dose gradients [1,2]. Based on the aforementioned issues and on [3] the following eleven requirements were identified for a motion management radiotherapy research phantom. (i) Represent a suitable anatomical site, such as thorax and abdomen, including realistic human anatomy and tissue equivalent material. (ii) Generate 3D translational and 3D rotational motion. (iii) Generate programmable regular motion to address the reproducibility of motion compensation and tracking strategies. (iv) Generate human-like trajectories with a naturally wide variability (period: [0.2, 0.3] Hz; amplitude: [3.9, 18.5] mm (SI), [0, 9.4] mm (AP) and [1, 10.5] mm (LR)[8]; velocity: [5, 15] $mm.s^{-1}$ and acceleration: [10, 25] $mm.s^{-2}$) [4,5,8] exhibiting both cyclic behaviour, with varying frequency as well as slow intra-fractional aperiodic trends which can be of greater magnitude than the cyclic signal [4-8]. (v) Generate both internal and external motion with programmable degrees of correlation and phase shift. (vi) Include deformable parts/components to evaluate the effect of organ/structure deformation on motion detection algorithms. (vii) Be compatible with commercial and research motion monitoring systems; (viii) Be 4DCT and MRI compliant. (ix) Have extendable I/O signal interfaces to trigger motion start or beam gate output. (x) Have the possibility to insert devices to measure the dose distribution received by the target and some surrounding tissues, e.g. ionisation chamber(s), film(s) or gel dosimeter. (xi) Be compact and easy to set up.

To date, there is no phantom that fulfils all these requirements, see [3, 9-13] and references therein. Most phantoms are platform based and not anthropomorphic focusing on ease of use and compactness [3, 9]. Others are much larger and exploit standard robotic manipulators to benefit from their inherent high accuracy when realising complex target motions [3, 14]. Some phantoms focus on the use of deformable structures to achieve accurate body structure densities [12,13]. The difficulty for phantoms using deformable material is to be able to generate a reproducible and accurate deformation. Despite the importance of rib motion in terms of high-density material interfering with the

beam path, only a few phantoms have a moving ribcage. By contrast with phantoms which achieve motion through deformation using pneumatic actuators, the MAESTRO thorax phantom, developed during the Framework 6 European integrated project on Methods and Advanced Equipment for Simulation and Treatment in Radiation Oncology (MAESTRO), , moves each set of ribs mechanically. It fulfils the requirements (i) to (xi) with the limitation that only 3D translational motion can be generated and that the insert should be sufficiently small to fit in either the left or the right lung. The moving rib cage addresses, to some extent, requirement (vi), however, it is not the lung volume that changes but the volume between the skin/ribs and the static lungs. A combination of natural sponge, Dermasol, nylon wires and Lucite beads similar to [13] could however be mechanically deformed within the static lung for more challenging imaging studies with realistic lung densities. The Material and Method Section describes the phantom design and the experimental methods adopted to study the phantom motion and its practical use. The results section focuses on the novel rib cage motion characteristics.

II Material and Methods

II.A Phantom design and components

The MAESTRO thorax phantom comprises two main components i) a motorised rib cage including eight sets of moving ribs, two stationary lungs, a trachea and a spine enclosed by a skin used to form a hermetic container which can be filled with water, leaving easy access to the lung cavities, see FIG 1 and FIG S1 in supplemental material; ii) a robotic arm which can apply 3D translational motion to a target within either the left or the right lung. The latter can be replaced by any other robotic device to generate the target motion or deform foam material within the static lungs. The phantom dimensions are: length (SI) 30 cm, width (LR) 32 cm, height (AP) increases from 18 cm at the superior end to 24 cm at the inferior end with a maximum of 45.5 cm high for the water overflow column added to allow for volume expansion during inhale-exhale phases. The dimension of the phantom enables it to fit in standard linac as well as in a ring based gantry e.g. CT, MRI and VERO^{TM}. The right and left lungs dimensions are SI 29 cm, LR 13 cm, AP 6 cm and SI 31 cm, LR 11 cm, AP 9 cm respectively. Target inserts include a film holder 6 cm diameter by 3 cm width and a build-up cap fitting in a cylinder 5 cm height and 3 cm diameter. However more elongated inserts could be used depending on the programmed motion given that the operating envelope is 13 cm SI by 6 cm AP by 6 cm SI.

A novel mechanism was developed to move the ribs. Each set of ribs pivots about a set of shaped plates (denoted 'P' in FIG. 1a and 1c) that are attached to the static frame of the phantom corresponding to the superior and inferior sides. The shaped plates were designed to allow each set of ribs to rotate synchronously with the upper ribs moving less than the lower ribs. The bottom parts of the ribs are fixed onto a frame using pivots. The frame is moved along the SI direction by a stepper motor (23HSX-306) fixed onto an overflow column (Fig. 1d). The relatively small motion of the frame is amplified according the distance between the pivot representing the centre of rotation and the bottom pivot attached to the tray. The motion of the ribs about the pivots results in both SI and AP motion with some residual LR motion see FIG 1a-c.

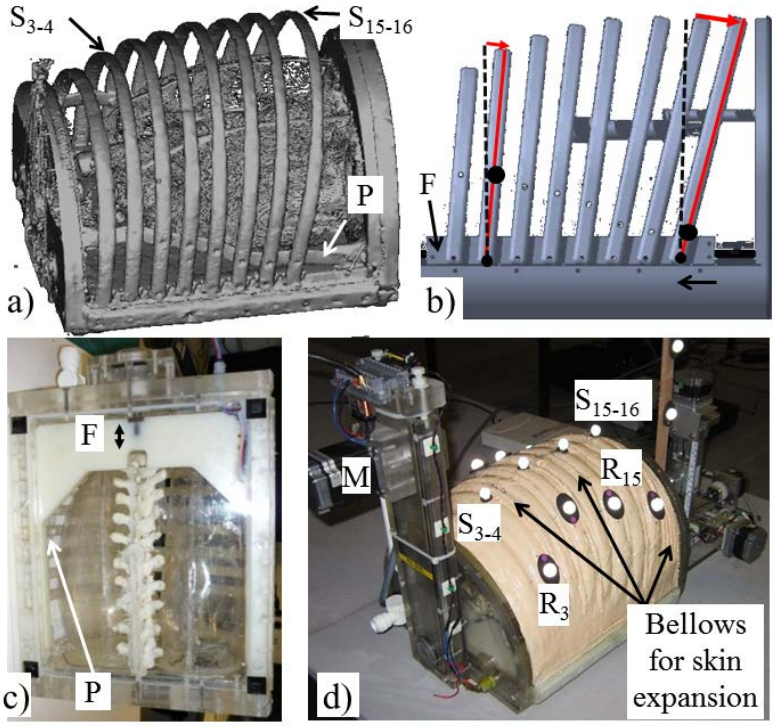

FIG. 1. MAESTRO thorax phantom rib motion mechanism: a) 3D CT study at exhale showing the shaped Perspex frame, denoted 'P', onto which the pivots are fixed; b) CAD diagram of the thorax illustrating the motion for ribs 3-4 and 15-16. The ribs, attached to the base of the frame (small black discs), rotate about the pivots (large black discs) due to the linear motion applied in the SI direction (see c). The dashed lines represent the centre position and the plain lines represent the exhale position. c) Bottom view of the phantom showing the Perspex frame moved by a stepper motor, denoted M in d), through a belt and screw mechanism to convert rotational to translational motion. d) Phantom with infrared markers tracked by the VICON Nexus system to characterise the ribs motion.

The bottom, front and rear of the phantom as well as the water expansion column are realized with Perspex. The skin is composed of latex reinforced with gauze. To prevent skin expansion due to the large volume of water contained within the phantom a 2 mm skin, shaped by painting latex onto gauze positioned onto a phantom cast, was sewn to each set of ribs. The skin bellows (see FIG 1d and S1b) were designed to accommodate ribs motion. The spine, ribcage, the inner spine and the cartilage were manufactured using 45, 31, 5.7 and 1.5 % of $CaCO_3$ (2.71 gcm^{-3}) mixed with Epoxy resin (1.07 $g.cm^{-3}$) respectively based on [17-19] and experimental verifications to adjust the compounds ratio.

To date three types of inserts have been used to perform dosimetric and motion studies. Wax blocks were used to insert thermo luminescent dosimeters (TLDs) or an ionization chamber. A film holder, attached to the slider system using two parallel rods was used to simulate and measure dose delivered to a moving target with and without motion compensation [15]. The film holder enabled the insertion of a 5 cm diameter film. A build-up cap was used to enable the installation of an ionization chamber and provide accurate point dosimetry, see FIG. 2 as well as position fiducial markers and assess their detection.

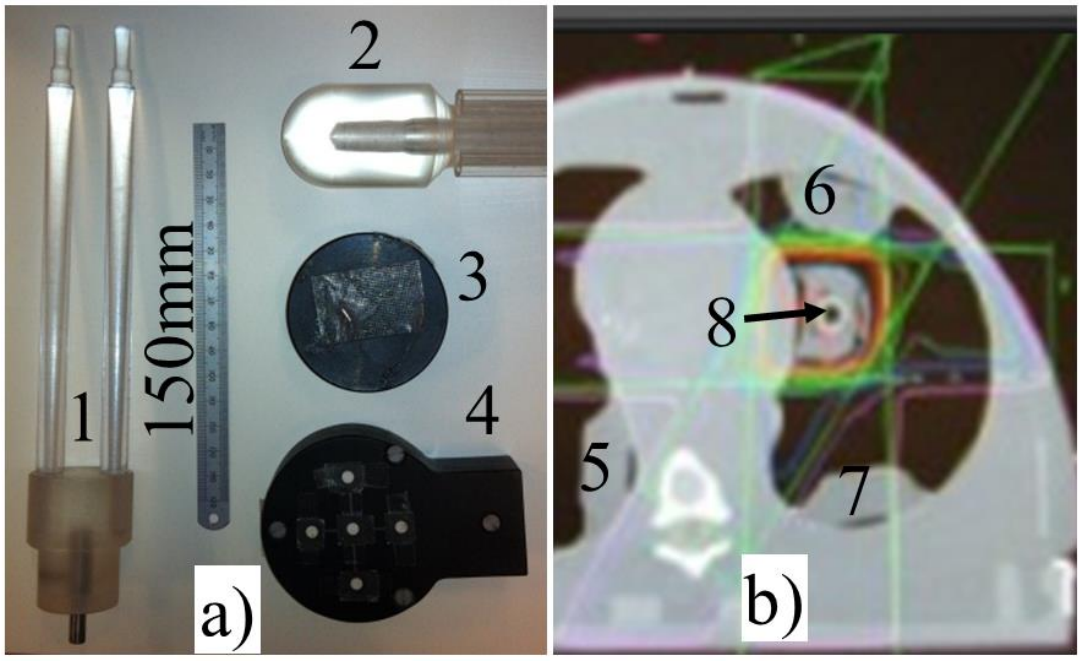

FIG. 2. Phantom inserts: a) 3D slide system attachment for lung inserts (1), ionisation chamber insert (2), inserts for 5cm diameter film (3,4); b) wax blocks for TLDs (5-7) or ionisation chamber (8).

The target motion system was constructed using three slides (Unislide, LG motion, Basingstoke, UK) supported by high precision linear rails and driven by a 23HSX-102 stepper motor via a lead screw. Gear boxes were added to the SI and AP directions in the ratio 1 to 3 and 1 to 2 respectively to accommodate the velocity and acceleration required. Position sensors were subsequently added onto each axis to (i) enable position feedback control and (ii) to synchronise the recording of position measured by the phantom and external devices. A Windows laptop-based open loop control system was developed using LabVIEW™ to drive each stepper motor through either a 6024E PCMICA card connected to a SC-2075 or a NI USB-6229 DAQ. The latter provides a large number of analogue and digital signals to synchronise the phantom with external systems. Each axis of motion of the 3D slide and the ribcage can perform different trajectories calculated based on mathematical models implemented in LabVIEW™, MATLAB®, Scilab or loaded from a file (ASCII text or spread sheet). The software re-samples and quantizes each trajectory to accommodate the velocity and acceleration limitations imposed by the phantom drive mechanism.

II.B Phantom motion evaluation

The phantom motion was evaluated using three different methods. Motion of the 3D slide system controlling the target motion was evaluated using a position sensor LIPS P 103, Positek Cheltenham, UK which exhibited fast response and a high accuracy (http://www.positek.co/Specs/p103spec.htm). Motion of the ribs at the locations denoted as $S_{15\text{-}16}$ in Fig. 1 was evaluated with the same sensor. Motion of the 2D slider driving the ribs was evaluated using an in-house video tracking system. The overall external 3D rib cage motion was evaluated using a VICON system (http://www.vicon.com/). The system used 12 VICON MX40 cameras with the VICON Nexus software v1.7 to capture images at 30Hz and determine the 3D position of 12 markers located in the middle section (sternum) as well as the left and right sides of the phantom ribcage, see FIG. 1d. The stated absolute accuracy was 0.5 mm; however, it is our experience that better relative accuracy can be achieved. The range of motion was obtained by moving the phantom manually between the maximum inhale and exhale positions. Motion linearity was evaluated by comparing the signals sent to the rib cage with that measured by the VICON or the LIPS P 103 position sensor fixed onto the set of ribs corresponding to location $S_{15\text{-}16}$. To illustrate the wide range of signals that can be programmed or loaded from file and accurately reproduced, a sinusoidal waveforms and an irregular motion based on a bilinear model [15, 20] were generated by the phantom and measured using the VICON system. The latter trajectory was then used to evaluate the ability of the rib cage and 3D target positioning system to produce arbitrary

motion for long periods of time. Motion reproducibility was evaluated by comparing measured motion in subsequent cycles. The root mean square error (RMSE) was calculated to characterize the difference between each cycle. The effect of the rib motion on the phantom geometry was evaluated by performing CT scans, with a TOSHIBA Aquilion/LB helical CT, at inhale and exhale positions. Pixel spacing was set to 1.0740 mm and slice thickness at 2 mm. The phantom skin outline was delineated and its area calculated for each CT image to visualise the effect of rib motion and compare the corresponding CT image at inhale and exhale. MATLAB and its Image Processing Toolbox V 8.2 were used to perform the automatic outlining and area calculation using a combination of edge detection and mathematical morphology.

III. Results

III.A Target inserts motion characteristics

The maximum ranges of motion of the sliders are 125 mm (SI), 88 mm (AP) and (LR), however when used in conjunction with the rib cage to move a target within one of the lungs, the range of motion is limited by the internal dimension of the lungs, see Section II. Such a large range is however useful to evaluate the effect of drift on motion management. The 3D slide resolutions are 0.016, 0.0050 and 0.015 mm/step and the maximum velocities are 16, 5, and 15 mm/s, at 1 kHz sampling frequency, for the AP, LR and SI directions respectively. Fig.3 illustrates the ability of the phantom to apply sinusoidal waveforms of different amplitude and phase shift concurrently. It exhibits an acceptable repeatability with RMSE between successive cycles in the range [0.1, 0.16] mm for the sinusoidal waveform compared to [0.003, 0.013] mm an the immobile marker There are no issues with the linearity of the slider, as the waveforms produced by the slider are identical to the one generated by the phantom control system. Similar findings were obtained for the third axis of motion (LR).

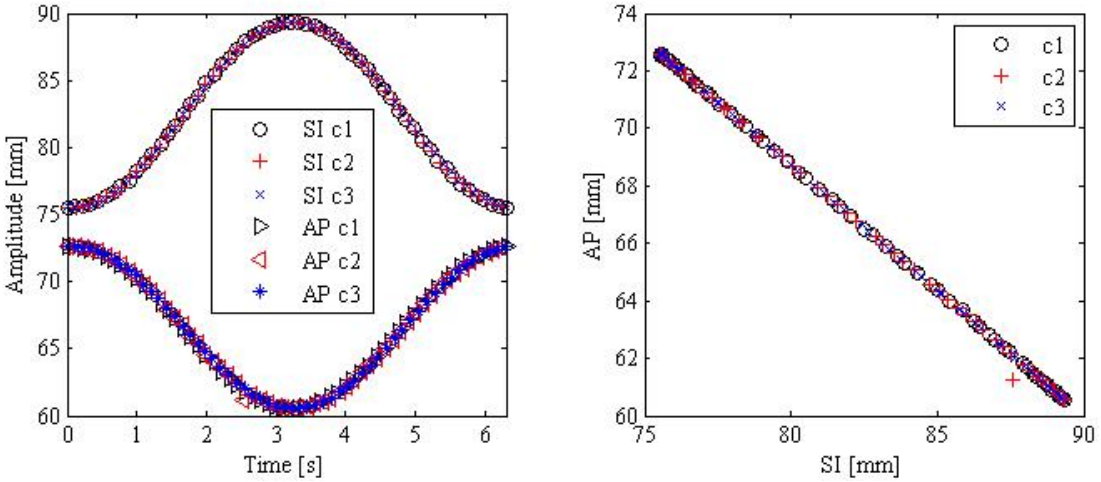

170 FIG. 3. 2D repeatability of the slider motion for AP and SI using a sinusoidal waveform with period 6.3s, SI amplitude 14 mm and AP amplitude 12 mm over three successive cycles c1, c2 and c3.

III.A Rib motion characteristics

175 The maximum amplitude of motion for each pair of ribs ranges from 7 to 20 mm in SI, and from 1 mm to just under 4 mm for AP with LR motion being of the order of 1 mm, see Table 1. In applications requiring larger amplitude in AP, the AP motion can be increased by converting some of the SI motion into AP motion by locating the phantom on an incline (4DCT commissioning) or fixing a flexible plastic film between the ribs $S_{15\text{-}16}$ and the frame of the phantom (experiment with VERO).

180 The relationship between the signal sent by the control system and the resulting ribs motion in SI and AP is slightly nonlinear due to the geometry of the pivot mechanism and the existence of some backlash, see FIG. 1. This nonlinear response results in flat topped slightly distorted triangular waveform for a triangular signal sent to the motor drive. The motion nonlinearity is consistent and not significantly affected by the speed of the ribs, see FIG. 4. To overcome the effect of backlash the velocity of the drive can be artificially increased, see sharp change of

185 direction achieved at 35 s in FIG. 4. The rib motion is reproducible and repeatable with RMSE between the first and successive cycles of a sinusoidal signal being of the order of 0.08 mm, see FIG. 5 and in the range [0.04, 0.16] mm for the signal shown in FIG 4.

TABLE I. Range of motion of the rib cage for sensor location indicated in Fig. 1d.

Motion [mm]	Marker location											
	S_{3-4}	R_3	R_4	S_{7-8}	R_7	R_8	S_{11-12}	R_{11}	R_{12}	S_{15-16}	R_{15}	R_{16}
SI	7.2	2.5	2.1	11.4	8.3	7.8	19.6	11.9	12.1	20.0	11.4	9.8
AP	0.9	0.8	0.9	0.5	0.6	0.7	2.6	2.2	1.4	3.7	2.3	2.0
LR	0.8	0.5	2.2	0.8	0.5	0.9	0.8	1.4	0.9	1.3	1.1	0.8

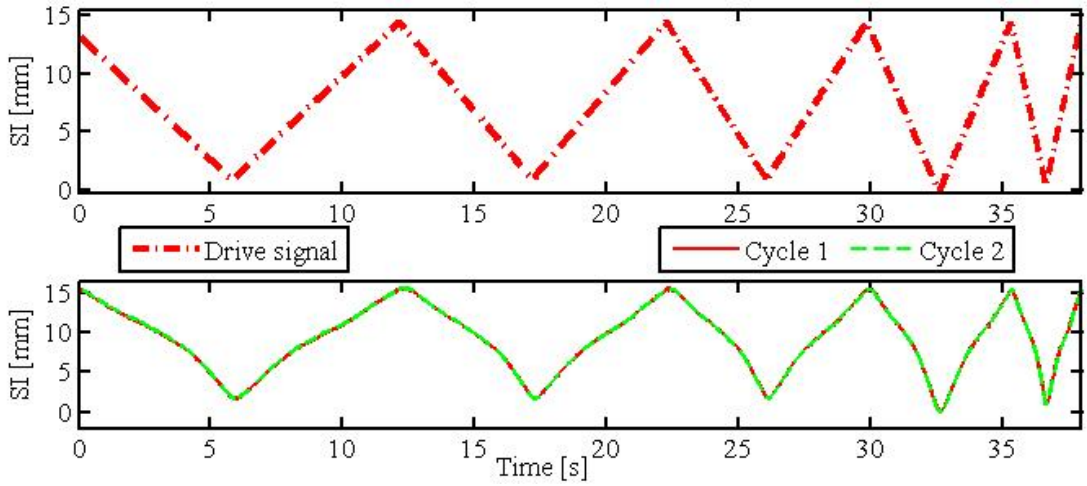

FIG. 4. Nonlinear relationship between the signal sent to the stepper motor to move the ribs and the main rib motion in SI: (Top) normalised input trajectory sent to the rib motor drive system; (bottom) resulting position measured by position sensor LISP P 103.

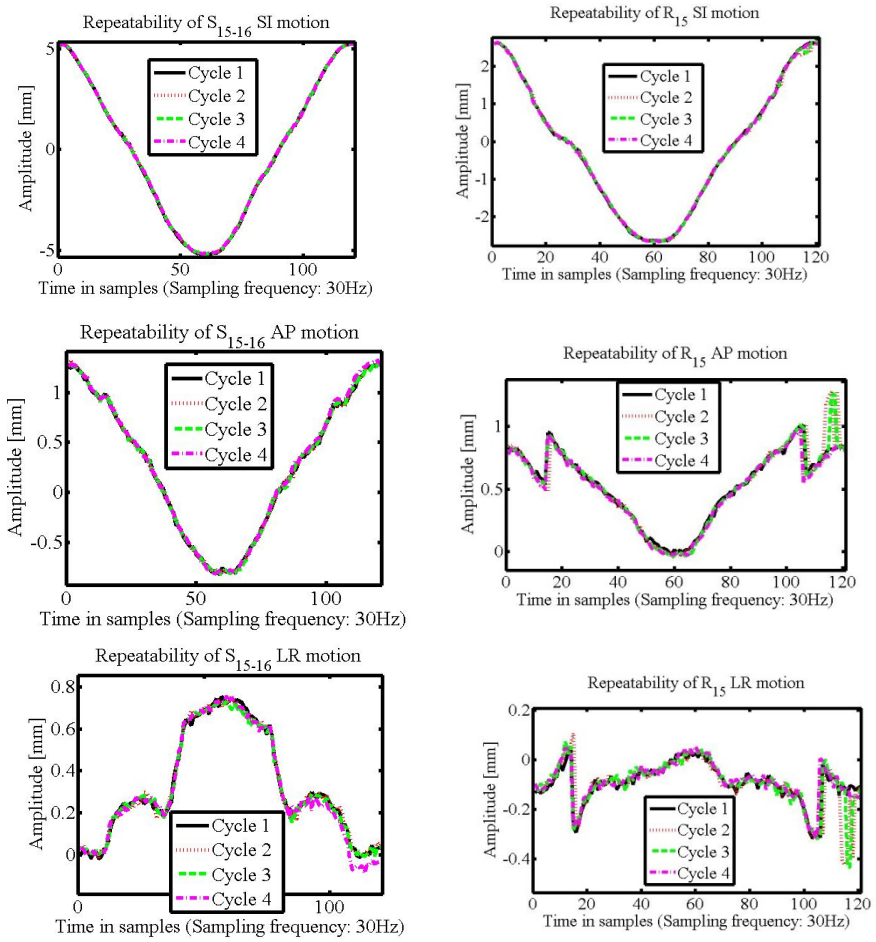

205

FIG. 5. Rib cage motion linearity and repeatability for markers located in $S_{15\text{-}16}$ (left column) and R_{15} (right column), see FIG. 1a. The correlation between SI and AP motion increases with the amplitude of motion and depends on the shape of the fixed plate supporting the pivots around which the ribs rotate. The location of the marker R_{15} near the pivot mechanism results in smaller amplitudes than observed for $S_{15\text{-}16}$.

210

The reproducibility of the rib cage motion for a statistically generated signal based on a bilinear model [20] is shown in Fig. 6a. The samples between 3000 and 500 correspond to the portion of the signal acquired by VERO™ using external markers (Fig 6b-d) to establish a correlation model with the fiducial marker position obtained by the kV X-

215 rays. This experiment demonstrated the simultaneous motion of the 3 axes of the target positioning system as well as the rib cage.

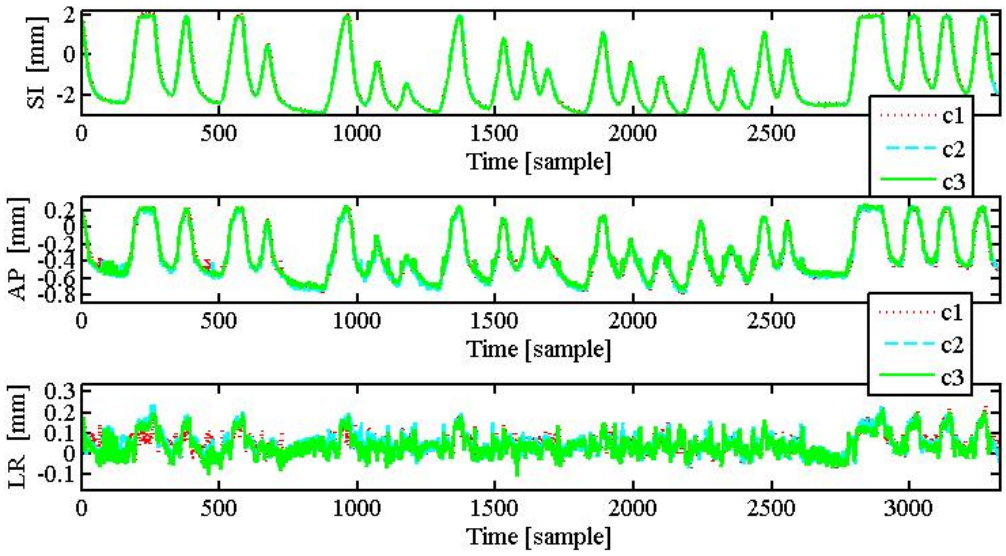

a) b) c) d)

FIG. 6. a) Irregular signal of varying period, amplitude and frequency generated by the phantom and measured (30 Hz sampling) at point $S_{15\text{-}16}$ using the VICON system (http://www.vicon.com/) for three successive repetitions (c1-c3). b-d) Extracts from the VERO 4D modelling module (pre-clinical version) showing a) motion correlation between external (cyan/light grey) and internal markers (orange/dark grey). b) External reflective markers located on the MAESTRO thorax phantom; c) Fiducial marker located on ionisation chamber insert monitored with kV-X-ray.

III.B Effect of rib motion on CT geometry

The ribs motions create a variation in the phantom volume which is visualised by the change in area of the phantom outline for corresponding CT slices between the inhale and the exhale phases. FIG 7 illustrates this process using the CT images, at inhale and exhale, at index position 141. It can be observed that differences in area are up to 5% (4th peak from the right in Fig. 7 top). The CT automatic outlining (FIG. 7 bottom) can be challenging due the skin contour blurring effect created by the skin bellows used to accommodate for rib cage expansion, see Section II and S1.2. The evaluation of more challenging image processing tasks such as non-rigid registration and tracking would require more realistic material for the lung insert using an approach similar to [12].

The CT image confirms the dosimetric accuracy of the substitute material with mean mass density and Hounsfield Unit for the cartilage (1.09 g.cm^{-3}, 96 HU), the ribcage (1.47 g.cm^{-3}, 472 HU), the spine hard bone (1.81 g.cm^{-3}, 698 HU) and spine inner bone 1.12 g.cm^{-3}, 164 HU), being within 3% of patient data, see Table S1 and S2 in Supplemental material.

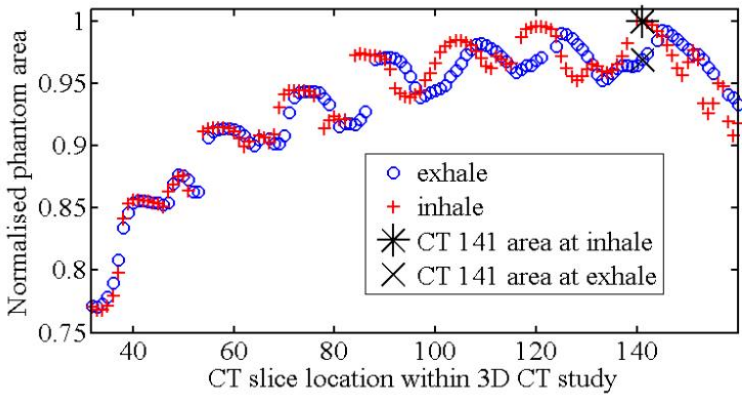

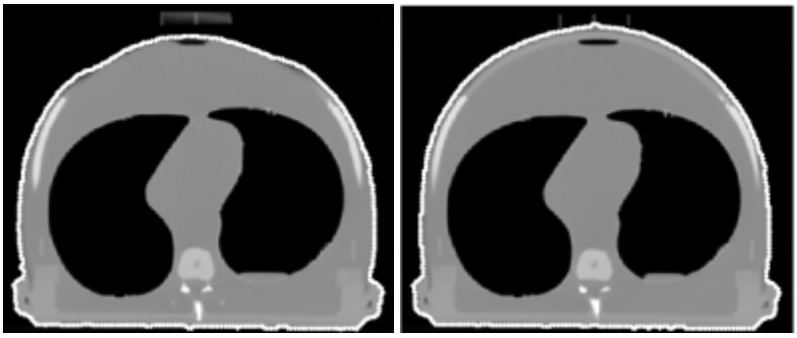

FIG.7 Effect of rib the motion on the area enclosed within the skin of the phantom: ‘o’ and ‘+’ represent the areas of the polygons obtained by contouring each CT image. The area enclosed within the outline of the CT images at inhale (bottom right) and exhale (bottom left) correspond to the points indicated by ‘×’ and ’∗’ (top). The different densities used to manufacture cartilage; ribs and spine are clearly identifiable together with the Perspex frame used to move the ribs.

IV. Summary

This paper has presented the MAESTRO thorax phantom, a new dynamic anthropomorphic phantom, for IGRT and ART, capable of replicating a wide range of realistic and independent 3D tumour and thorax motion. The ribcage motion is produced with a single actuator driving the SI motion, however the new rib design enables it to produce SI, AP and to a lesser extent LR motion. The new design enables each set of ribs to pivot about a frame shaped to produce individualised amplitude of motion. A specialist 3D tracking system was used together with a 1D position sensor and CT studies at inhale and exhale to assess the overall 3D rib motion. It was found that the maximum ranges of ribs motion are SI 20 mm, AP 3.7 mm and LR 1.3 mm. The upper ribs motion are 3 to 4 times smaller than

that of the lower ribs in term of SI and AP respectively. The relationship between SI and AP is approximately linear for ribs with large amplitude of motion. The rib construction leads to a slightly nonlinear response between the drive signal and the SI motion, the latter can however be linearized programmatically. The new rib cage design can deliver deterministic and reproducible rib motion. Each element of the phantom has been evaluated dosimetrically and found to be in good agreement in terms of tissue equivalence. To date the phantom has enabled the demonstration of couch motion compensation and the evaluation of different types of fiducial markers for motion correlation on an early prototype of the VERO tracking system. It is currently used for 4D CT commissioning at UHCW.

Acknowledgement:

This work was sponsored by Framework 6 European integrated project Methods and Advanced Equipment for Simulation and Treatment in Radiation Oncology CE LSHC CT 2004 503564. The Authors are grateful to the staff of the Radiotherapy Departments at the University Hospital, Coventry, UK. We would also like to acknowledge Brainlab for facilitating access to a VERO prototype. Finally I would like to acknowledge Laure Bousselin and François Coipeault, placement students from ESEO Institute of Science and Technology, France for their help in developing the image processing routines to analyse the CT images and the phantom performance.

[1]K.M. Kraus, E. Heath, U. Oelfke, "Dosimetric consequences of tumour motion due to respiration for a scanned proton beam," Phys. Med. Biol. **56**(20), 6563-6581 (2013).

[2]J.J. Sonke, J. Lebesque, M. van Herk, "Variability of Four-Dimensional Computed Tomography Patient Models," Int. J. Radiat. Oncol., Biol., Phys. **70**(2), 590-598 (2008).

[3] P. Steidl, D. Richter, C. Schuy, E. Schubert, T. Haberer, M. Durante, and C. Bert, "A breathing thorax phantom with independently programmable 6D tumour motion for dosimetric measurements in radiation therapy," Phys. Med. Biol. **57**(8), 2235–50 (2012).

[4] R. George, T. Chung, S. Vedam, V. Ramakrishnan, R. Mohan, E. Weiss and P. Keall, "Audiovisual biofeedback for respiratory-gated radiotherapy: Impact of audio instruction and audio-visual biofeedback on respiratory-gated radiotherapy," Int. J. Radiat. Oncol. Biol. Phys. **65**(3), 924–933 (2006).

[5]S. Quirk, N. Becker, W.L. and Smith, "External respiratory motion analysis and statistics for patients and

volunteers," Journal of Applied Clinical Medical Physics, **14**(2) Mar. 2013.

[6] D. Verellen, M. De Ridder, and G. Storme, "A (short) history of image-guided radiotherapy," Radiother. Oncol. **86**(1), 4–13 (2008).

[7] M.J. Murphy, Tracking organs in real time, Seminars in Radiation Oncology **14** (1), 91–100 (2004).

[8] PJ Keall, GS Mageras, JM Balter, RS Emery, KM Forster, SB Jiang, JM Kapatoes, DA Low, MJ Murphy, BR Murray, CR Ramsey, MB Van Herk, SS Vedam, JW Wong, E.Yorke "The management of respiratory motion in radiation oncology report of AAPM Task Group 76," Med Phys. **33**(10) 3874-900 (2006).

[9] M. Schaefer, M. W.Munter, C. Thilmann, F. Sterzing, P. Haering, S. E. Combs, J. Debus, "Influence of intra-fractional breathing movement in step-and-shoot IMRT," Phys. Med. Biol. **49**(12), 175–9 (2004)

[10] T. Zhou, J. Tang, S. Dieterich, and K. Cleary, "A robotic 3-D motion simulator for enhanced accuracy in CyberKnife stereotactic radiosurgery," in *CARS*, edited by H.U. Lemke, K. Inamura, K. Doi, M.W. Vannier, A.G. Farman and J.H.C. Reiber (Elsevier), 323–328 (2004).

[11] E. Nioutsikou, J.R.N. Symonds-Tayler, J.L. Bedford, and S. Webb, "Quantifying the effect of respiratory motion on lung tumour dosimetry with the aid of a breathing phantom with deforming lungs," Phys. Med. Biol. **51**(14), 3359 (2006).

[12] J. Chang, T.-S. Suh, and D.-S. Lee, "Development of a deformable lung phantom for the evaluation of deformable registration". Journal of Applied Clinical Medical Physics **11**(1), 281-286 (2010).

[13]M. Serban, E. Health, G. Stroian, D. Louis Collins and J. Seuntjens, A deformable phantom for 4D radiotherapy verification: Design and image registration evaluation," Med Phys. **35**(3), 1094–102 (2008).

[14]J. Wilbert *et al.*, "Tumor tracking and motion compensation with an adaptive tumor tracking system (ATTS): System description and prototype testing," Med Phys. **35**(9), 3911–3921 (2008).

[15] O.C.L. Haas, P. Skworcow, D. Paluszczyszyn, A. Sahih, M. Ruta, and J.A. Mills, "Couch-based motion compensation: modelling, simulation and real-time experiments," Phys. Med. Biol. **57**(18), 5787–807 (2012).

[16] T. Depuydt, D. Verellen, O. Haas, T. Gevaert, N. Linthout, M. Duchateau, K. Tournel, T. Reynders, K. Leyse, M. Hoogemanc, G. Storme. M. De Ridder, "Geometric accuracy of a novel gimbals based radiation therapy tumor tracking system," Radiother. Oncol. **98**(3), 365–372, (2011).

[17] D. R. White, C. Constantinou, and R. J. Martin, "Foamed epoxy resin-based lung substitutes," British Journal of Radiology, **59**(704), 787-90 (1986)

[18] U. Schneider, E. Pedroni, and A. Lomax, "The calibration of CT Hounsfield units for radiotherapy treatment planning," Phys. Med. Biol., **41**(1), 111-24 (1996).

[19] S.J. Thomas, "Relative electron density calibration of CT scanners for radiotherapy treatment planning," Br. J. Radiol. **72(**860), 781-6 (1999)

[20] A. Sahih, O.C.L. Haas, J.H. Goodband, D. Putra, J.A. Mills, K.J. Burnham, "Respiratory motion prediction for Adaptive radiotherapy," IAR 2006 November 16-17, Université Henri Poincaré, Nancy, Fr, www.acd-2006.cran.uhp-nancy.fr/Files/IAR/p14.pdf (2006).

Supplemental material

S1.1 Phantom components

a) Internal structure of the phantom lungs, trachea, vertebrae and spine

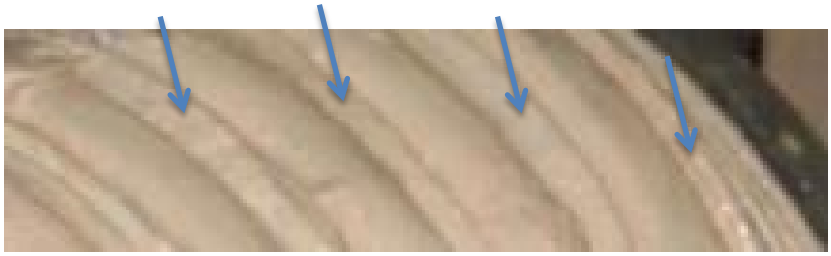

b) illustrating the use of bellows to allow for skin expansion

FIG. S1.

S1.3 Linearity and reproducibility of slider motion

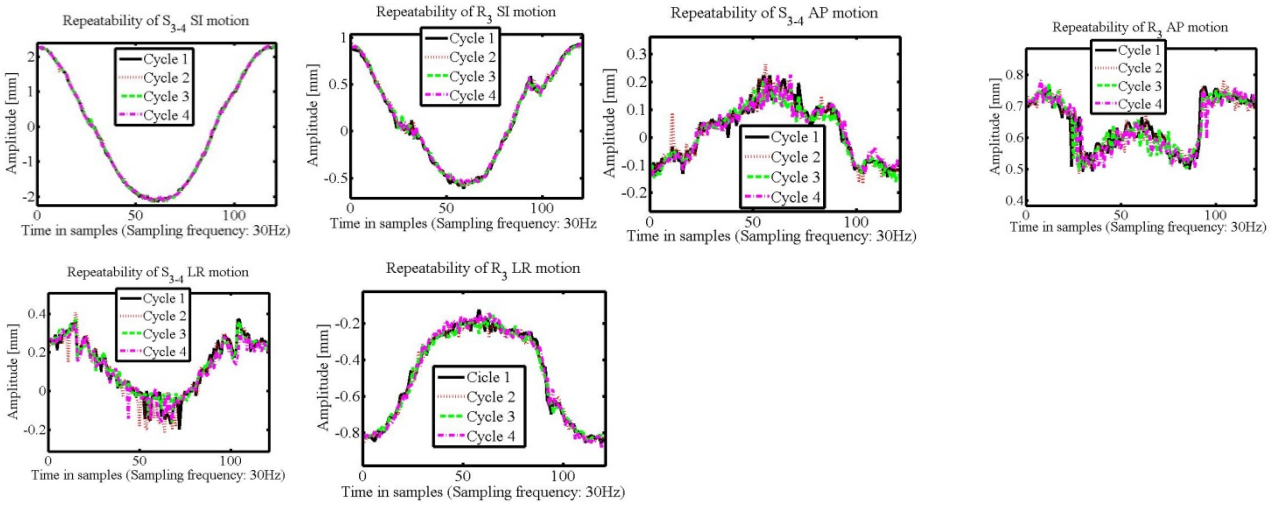

335 FIG. S2 Illustrating the repeatability of motion for a given marker location on the rib and the relationship between motion in AP, SI and LR. The degree of correlation between SI and AP motion increases with the amplitude of motion and depends on the shape of the fixed plate supporting the pivots around which the ribs rotate, see Fig. 1f. The location of the markers R3 and R15 near the pivot mechanism results in smaller amplitudes than the markers S3-4 and S14-15 located on top of the phantom.

340

S1.3 Dosimetric study

Skin and bone substitutes were initially evaluated for dosimetric fidelity. Skin was compared to epoxy-resin-based solid water.

Bone substitutes were compared to the materials describe in references 16 – 19 and patients' CT. Two types of CT studies were then realised. Initially the entire treatment process for the whole phantom was then simulated to identify the accuracy between calculated dose and delivered dose to the phantom. The process was as follows: 1) Scan the thorax phantom (General Electric Lightspeed CT scanner). 2) Plan two standard treatments to calculate the dose at key locations within the phantom (XVplan® treatment planning system). 3) Deliver a dose of 200 cGy per fraction to the middle of the gross tumour volume (GTV) using 6 MV photons from two Elekta linacs. 4) Measure the dose using a combination of a 6 MV build-up cap for an ionisation chamber representing the target in the middle of the left lung and three wax blocks inserted at different positions within the lung (see Fig. S2). Two thermoluminescent detectors (TLDs) were placed in each wax block. Blocks 1 to 3 enabled the positioning of two TLDs located at 1.5 cm either side to the centre of the target. Block 4 contained the ionisation chamber, one TLD placed anterior to the chamber and the other TLD posterior to the chamber at the isocenter position. The doses calculated by the TPS were then compared to the point doses measured in the phantom. The second CT study was aimed to evaluate the phantom motion as seen from the CT scanner and is described in the following sub-section.

A dosimetric study was carried out to evaluate differences in the scattering and attenuation properties of the latex used for the phantom skin compared to human tissue. Standard epoxy resin based solid water was used as the substitute material of reference for soft tissue. The central axis depth dose curves for solid water and the latex were measured at a source to skin surface distance (SSD) of 100 cm for a 6 MV and a 25 MV photon beam with a 8 cm by 8 cm field size. For all measurements an ionisation chamber was placed in a slab of solid water at a depth of 1 cm. Slabs of solid water or latex were placed on top of the chamber slab for comparative measurements in the beam. Slabs with 6 layers of gauze between the latex were manufactured to investigate the dosimetric effect of having gauze in some parts of the phantom skin. Both sets had a dimension of 10 cm by 10 cm. The following series of depth dose measurements were made: i) several thicknesses of solid water between 2 and 8 cm, ii) Several thicknesses of latex between 2 and 4.5 cm, iii) Several thicknesses of latex (between 2 and 4.5 cm) with 2 cm and 3 cm of solid water on top to move the latex slabs out of the build-up region for 6 MV and 25 MV photons

respectively, iv) several thicknesses of latex with added gauze between 2.5 and 5 cm, v) Several thicknesses of latex with added gauze (between 2.5 and 5 cm) with 2 cm and 3 cm of solid water on top to move the latex slabs out of the build-up region for 6 MV and 25 MV photons respectively. Measurements were repeated three times for each set-up.

Results

The observed discrepancy in bone electron density is well within the variability that can be observed on patients' CT. Considering the mean value only, the observed discrepancy would lead to dosimetric errors of less than 0.5%, confirming the acceptability of the bone substitute materials. The dosimetric discrepancy for the skin material was within ±0.5% for 6 MV photons and ±1.0% for 25 MV photons. A t-test at 95% confidence level was applied and indicated that there were no significant differences ($P>0.05$) in the mean values for all measurements.

The whole-thorax dosimetric evaluation showed good agreements between the measured and calculated. TLD measurements were compared to calculated dose target giving maximum errors ranging from -2.69 % to 1.16% when the targets were located on the side of the lungs, see Table S3 in supplemental information. This was due to the difficulty in accurately re-positioning the target in the side of the lung compared to the middle of the lung. When target was positioned in the middle of the lung with the 3D slide system with maximum errors was reduced 1.06%, see Table S4 in supplemental information. In all cases the dosimetric evaluation met the designated target of ±3%.

TABLE S1. Comparison between the mass density for the substitute material using data from ICRU Report 44 (ICRU 1989) and data found in the literature e.g.*White et al [17], +Schneider et al[18]. Composition in % of weight for different bone substitute materials. The epoxy resin with hardener mixing ratio of 100:40 by weight

Tissue (bone) type	Mass density in [g.cm−3]			Composition % weight	
		ICRU Report 44	Substitute	CaCO3	Epoxy resin
Spine - inner bone	1.12*	1.03	1.13	5.7	94.3
Spine - hard bone	1.85*	1.92	1.81	45.0	55.0
Ribcage	1.41 to 1.52+	—	1.47	31.0	69.0
Cartilage	—	1.10	1.09	1.5	98.5

TABLE S2. Substitute material HU, patients CT scans and a CT electron density phantom for different bone types; mean and standard deviation on 20 samples.

Type	HU (mean ± σ deviation)		
	substitute	patients CT scans	electron density phantom
Spine - inner bone	164 ± 24	167 ± 43	239
Spine - hard bone	698 ± 43	692 ± 131	263, 1202
Ribcage	472 ± 32	492 ± 183	263, 1202
Cartilage	96 ± 3	102 ± 41	

TABLE S3**.** Dosimetric measurements with ionisation chamber for a target at the side of left lung.

Plan	Machine	No. of set-ups	% Average absolute deviation	% σ	% Range
3 field	H1	4	2.31	0.53	-2.69, -1.44
3 field	L1	4	2.55	0.02	-2.57, -2.53
Spine	H1	4	1.07	0.13	-1.16, -0.97

TABLE S4. Dosimetric measurements with ionisation chamber for a target in the middle of the lung

Plan	Machine	No. set-ups	% Average Abs. dev.	% σ	% Range
3 field	H1	4	0.71	0.29	0.37, 1.06
3 field	L1	4	0.47	0.21	-0.68, -0.03
spine	H1	4	0.44	0.22	-0.45, 0.08

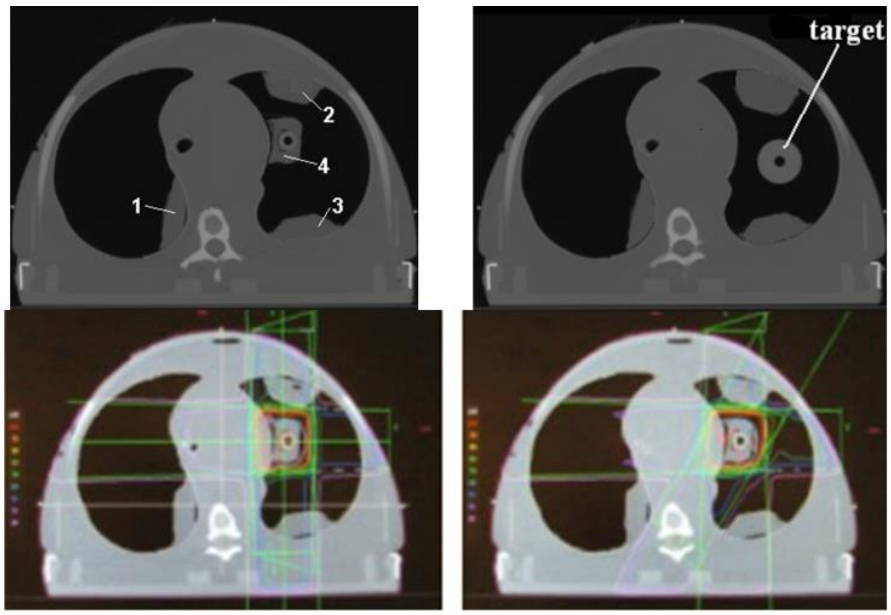

Fig. S2. Top: CT scans of thorax phantom, positions marked 1-3 indicate location of TLD and ‘Target’ in left side of lung being the insert or build up cap connected to the 3D slide system. Bottom: treatment plan obtained with XVplan corresponding to the situation illustrated in top left, left) 3 field plan, right) spine plan. The first plan (‘3 field plan’) represents a typical treatment plan used for lung tumours and consisted of a parallel opposed beam pair with wedges and a lateral beam, Fig 2 (bottom-left). The second treatment plan (‘spine plan’) involves a posterior beam that passes through the spine, Fig. S2 (bottom-right).